

# Common architecture of the flagellar type III protein export apparatus and F- and V-type ATPases

Tatsuya Ibuki<sup>1</sup>, Katsumi Imada<sup>1,2</sup>, Tohru Minamino<sup>1,3</sup>, Takayuki Kato<sup>1</sup>, Tomoko Miyata<sup>1</sup> & Keiichi Namba<sup>1</sup>

The proteins that form the bacterial flagellum are translocated to its distal end through the central channel of the growing flagellum by the flagellar-specific protein export apparatus, a family of the type III protein secretion system. FliI and FliJ are soluble components of this apparatus. FliI is an ATPase that has extensive structural similarity to the  $\alpha$  and  $\beta$  subunits of  $F_0F_1$ -ATP synthase. FliJ is essential for export, but its function remains obscure. Here we show that the structure of FliJ derived from *Salmonella enterica* serovar Typhimurium is remarkably similar to that of the two-stranded  $\alpha$ -helical coiled-coil part of the  $\gamma$  subunit of  $F_0F_1$ -ATP synthase and that FliJ promotes the formation of FliI hexamer rings by binding to the center of the ring. These results suggest that the type III protein export system and F- and V-type ATPases share a similar mechanism and an evolutionary relationship.

The bacterial flagellum is an organelle for motility, consisting of a rotary motor and a filamentous helical propeller. It is a macromolecular complex that comprises about 30 different proteins, with copy numbers per flagellum ranging from a few to a few tens of thousands<sup>1</sup>. The assembly of the flagellum starts from the basal body MS ring, which is a 24-nm rotor ring composed of 26 copies of FliF and spanning the cytoplasmic membrane<sup>1,2</sup>. To form the filamentous part of the flagellum, the subunit proteins are translocated into the central channel of the growing flagellum and to the distal end for self-assembly by the flagellar-specific protein export apparatus<sup>1,2</sup>. The export apparatus contains six integral membrane proteins (FlhA, FlhB, FliO, FliP, FliQ and FliR) and three soluble proteins (FliH, FliI and FliJ)<sup>3</sup>. The membrane subunits are thought to form a proton-driven export gate within the putative central pore of the MS ring to facilitate the unfolding and translocation of export substrates<sup>4,5</sup>. The soluble components promote the export process by binding and delivering export substrates to the export gate. To do this, they dock to its platform, which comprises the cytoplasmic domains of the membrane components, and they also help the substrates to enter the gate<sup>4,6</sup>.

FliI is a Walker-type ATPase<sup>7,8</sup> and shows extensive structural similarity with the  $\alpha$  and  $\beta$  subunits of  $F_0F_1$ -ATP synthase<sup>9</sup>. FliI exerts its full ATPase activity when it assembles into a homohexamer ring and is thought to form the ring when it binds to the platform of the export gate<sup>10,11</sup>, which is formed by the cytoplasmic domains of FlhA and FlhB. FliH not only suppresses the ATPase activity and oligomerization of FliI in the cytoplasm by forming the FliH<sub>2</sub>-FliI complex<sup>12,13</sup> but also promotes the docking of FliI onto the platform<sup>14</sup>. FliJ is essential for efficient export, although it is not essential for export itself because occasional flagellar formation is observed in its absence<sup>5,15</sup>. As FliJ interacts with flagellar axial proteins and prevents their premature aggregation in the cytoplasm, FliJ has been postulated to be a general chaperone for export substrates<sup>15</sup>. FliJ also binds to the FliH<sub>2</sub>-FliI complex and to the export gate proteins

FlhA and FlhB, which suggests that the FliH-FliI-FliJ complex delivers export substrates to the export gate upon binding to the FlhA-FlhB platform<sup>16,17</sup>. FliJ interacts with FliM, a C-ring component of the flagellar basal body<sup>18</sup>, and with export substrate-specific chaperones, such as FliT and FlgN<sup>19,20</sup>. In addition, FliJ enhances an interaction between the FliT-FliD chaperone-substrate complex and the N-terminal half of the C-terminal cytoplasmic domain of FlhA (FlhA<sub>C</sub>)<sup>21</sup>. FlhA<sub>C</sub> forms part of the FlhA-FlhB platform and comprises four compactly folded domains and a long, flexible linker connecting them to the transmembrane domain<sup>22</sup>. So the FliJ-mediated binding of chaperone-substrate complexes to a specific surface of the domains of FlhA<sub>C</sub> is likely to be a crucial step for the efficient delivery of substrate to the export gate. Thus, FliJ seems to regulate the entire export process through dynamic interactions with its binding partners. However, it remains unknown how these reactions proceed in the cell owing to a lack of structural information regarding the entire export apparatus. Even the structure of a complex composed of soluble components would be of great help in obtaining insights into the mechanism of export substrate delivery.

We therefore carried out structural analysis of FliJ from *S. enterica* serovar Typhimurium by X-ray crystallography, and studied its interactions with FliI by electron microscopy and biochemistry. We show that the FliJ structure was remarkably similar to part of the  $\gamma$  subunit of  $F_0F_1$ -ATP synthase and that FliJ promoted the formation of FliI hexamer rings by binding to the center of the ring. We discuss possible roles of FliJ in flagellar protein export and an evolutionary relationship between the type III protein export system and F- and V-type ATPases.

## RESULTS

### Crystal structure of FliJ

FliJ is a small protein with 147 residues. The strong tendency of FliJ to aggregate made it difficult to crystallize, but the three residues

<sup>1</sup>Graduate School of Frontier Biosciences, Osaka University, Osaka, Japan. <sup>2</sup>Department of Macromolecular Sciences, Graduate School of Sciences, Osaka University, Osaka, Japan. <sup>3</sup>Precursory Research for Embryonic Science and Technology (PRESTO), Japan Science and Technology Agency, Kawaguchi, Saitama, Japan. Correspondence should be addressed to K.I. (kimada@chem.sci.osaka-u.ac.jp) or K.N. (keiichi@fbs.osaka-u.ac.jp).

Received 15 July 2010; accepted 17 November 2010; published online 30 January 2011; doi:10.1038/nsmb.1977



**Table 1** Data collection and refinement statistics

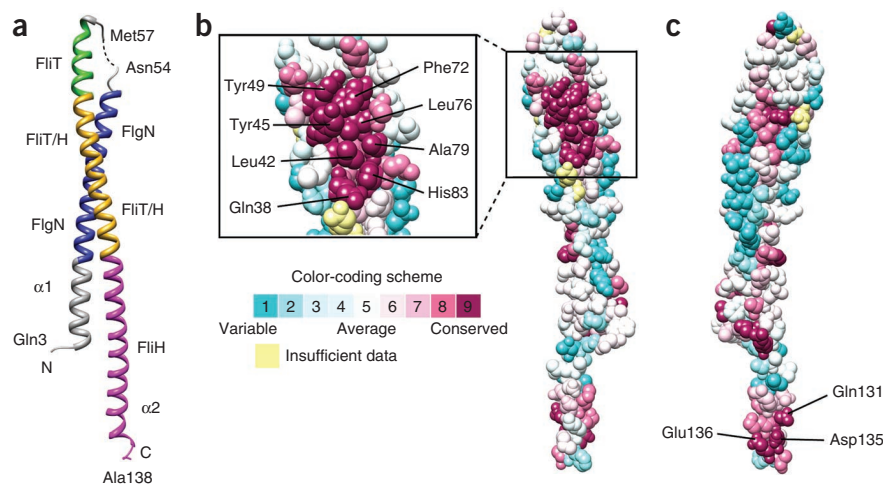
	FliJ mercury derivative
<b>Data collection</b>	
Space group	$P6_522$
Cell dimensions	
<i>a</i> , <i>b</i> , <i>c</i> (Å)	52.9, 52.9, 192.6
$\alpha$ , $\beta$ , $\gamma$ (°)	90, 90, 120
Resolution (Å)	2.1 (2.21–2.1)
$R_{\text{merge}}$	8.0 (31.7)
$I / \sigma I$	4.7 (2.2)
Completeness (%)	99.7 (100)
Redundancy	10.9 (11.1)
<b>Refinement</b>	
Resolution (Å)	37.3–2.1
No. reflections	10,032
$R_{\text{work}}/R_{\text{free}}$	23.3/25.5
No. atoms	
Protein	1,107
Ligand/ion <sup>a</sup>	1
Water	158
<i>B</i> -factors	
Protein	36.8
Ligand/ion	32.1
Water	52.6
R.m.s. deviations	
Bond lengths (Å)	0.005
Bond angles (°)	1.0

Values in parentheses are for highest-resolution shell. One crystal was used per dataset.  
<sup>a</sup>Ligand/ion is single mercury atom.

Gly-Ser-His attached to its N terminus as a histidine (His)-tag stub made it highly soluble and allowed crystallization<sup>23</sup>. We solved the structure using single anomalous diffraction data from its mercury derivative (Table 1). We built an atomic model of FliJ that contained residues from Gln3 to Ala138 except for Thr55 and Asp56 and refined it to 2.1 Å resolution (Fig. 1a). The electron densities for Thr55 and Asp56, the N-terminal five residues including GSH<sup>23</sup> and the C-terminal nine residues were not well defined.

FliJ adopted an antiparallel coiled-coil structure composed of two long  $\alpha$ -helices,  $\alpha 1$  and  $\alpha 2$ . Helix  $\alpha 1$  was eight turns shorter than helix  $\alpha 2$ , and hence the N- and C-terminal segments of  $\alpha 2$  protruded from the coiled-coil core. The FlgN- and FliT-binding regions<sup>19</sup> covered the C-terminal two-thirds of  $\alpha 1$  and the N-terminal half of  $\alpha 2$ , respectively. The FliH-binding region<sup>17</sup> extended over almost all of  $\alpha 2$  except for the first three turns and overlapped with the FliT-binding region in the middle of  $\alpha 2$  (Fig. 1a).

**Figure 1** Structure of FliJ. (a)  $C\alpha$  ribbon drawing of FliJ. The binding regions for FlgN, FliT, FliH and both FliT and FliH are highlighted in blue, green, magenta and yellow, respectively. (b,c) Evolutionarily conserved residues of FliJ. The figures were prepared by ConSurf (<http://consurf.tau.ac.il/>)<sup>36</sup>. Residues are colored in accordance with conservation among amino acid sequences of FliJ from 50 different bacterial species. (c) The back view of b.



Highly conserved residues among FliJ homologs were located on two exposed surfaces of the FliJ structure (Fig. 1b,c). One was between the C-terminal region of  $\alpha 1$  (38–49) and the N-terminal region of  $\alpha 2$  (72–83) and was formed mainly by hydrophobic residues. The other was formed by three hydrophilic residues, Gln131, Asp135 and Glu136, on the C-terminal, single-helical region of  $\alpha 2$ .

### Comparison of FliJ with the $\gamma$ subunit of $F_1$ -ATPase

Although the antiparallel,  $\alpha$ -helical, coiled-coil structure of FliJ seems to be a general motif found in many protein structures, when we used the DALI server<sup>24</sup> to compare the atomic coordinates of FliJ with structures in the Protein Data Bank, we found a strong similarity between FliJ and the  $\gamma$  subunit of  $F_1$ -ATPase, which was ranked in the top ten of the list. The structure of FliJ showed marked similarity to the coiled coil formed by the N- and C-terminal  $\alpha$ -helices of the  $\gamma$  subunit of  $F_1$ -ATPase<sup>25,26</sup> (Fig. 2). The lengths of their coiled coils and of each helix were comparable. Although the coiled coil of FliJ extends relatively straight, that of the  $\gamma$  subunit is bent around residue 24 in the N-terminal helix and residue 234 in the C-terminal helix. Therefore the whole FliJ structure could not be superimposed well onto that of the  $\gamma$  subunit. However, when the structure was divided into two regions at the bending point, the upper and lower parts of FliJ and the  $\gamma$  subunit superimposed nicely onto each other. The r.m.s. deviation between their upper regions (residues 26–45 and 65–98 of FliJ and residues 25–44 and 200–233 of the  $\gamma$  subunit) was 1.9 Å and that between their lower regions (residues 6–25 and 99–136 of FliJ and residues 5–24 and 234–271 of the  $\gamma$  subunit) was 1.6 Å for corresponding  $C\alpha$  atoms. The bending of the coiled coil of the  $\gamma$  subunit seemed to be caused by the interaction with its own  $\alpha/\beta$  domain. The C-terminal  $\alpha$ -helix of the  $\gamma$  subunit was bent along the  $\alpha/\beta$  domain, and the N-terminal  $\alpha$ -helix, the coiled-coil partner, was also bent accordingly. In the crystal structure of  $V_1$ -ATPase at 4.5-Å resolution<sup>27</sup>, the coiled-coil region of the D subunit, the central stalk of  $V_1$ -ATPase, was straight and its conformation appeared to be closer to that of FliJ than the  $\gamma$  subunit.

Although we found no apparent sequence similarity between FliJ and the  $\gamma$  subunit, structure-based sequence alignment revealed a region that was conserved between them (Fig. 2c,e). The conserved residues were located on the and interacted with the  $\epsilon$  subunit of  $F_1$ -ATPase<sup>26</sup> (Fig. 2d), which suggests that FliJ might have binding partners that correspond to the  $\epsilon$  subunit.

### FliJ affects the hexameric ring formation of FliI

The structural similarities between FliJ and the  $\gamma$  subunit shown here and between FliI and the  $\alpha/\beta$  subunits<sup>9</sup> suggested that FliJ and FliI

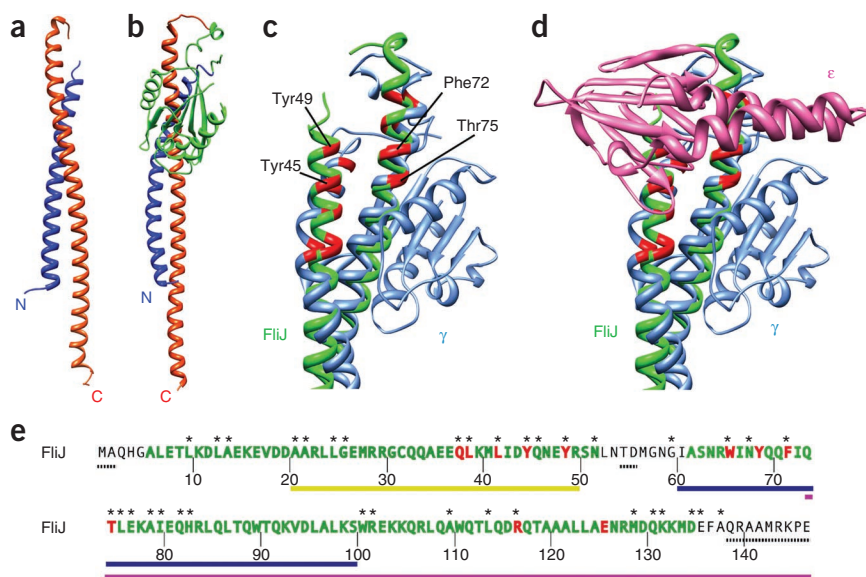


**Figure 2** Structural similarity between FliJ and the  $\gamma$  subunit of  $F_1$ -ATPase. (a,b)  $C\alpha$  ribbon drawing of FliJ (a) and the  $\gamma$  subunit of bovine mitochondria  $F_1$ -ATPase (PDB ID code 1E79)<sup>26</sup> (b). The  $\alpha$ 1 and  $\alpha$ 2 helices and the  $\alpha/\beta$  domain of the  $\gamma$  subunit are colored blue, red and green, respectively. (c,d) Close-up view of the conserved region between FliJ and the  $\gamma$  subunit. FliJ (green) is superimposed on the  $\gamma$  subunit (light blue). Residues that are highly conserved among FliJ homologs and  $\gamma$  subunits are shown in red. (d) The  $\epsilon$  subunit (pink; PDB ID code 1E79)<sup>26</sup> is displayed with FliJ and the  $\gamma$  subunit. (e) The amino acid sequence of FliJ with various information. Green characters denote  $\alpha$ -helices. Residues that are highly conserved between FliJ and the  $\gamma$  subunit are shown in red. The FliN-, FliI- and FliH-binding regions are shown by yellow, blue and purple bars below the sequence, respectively. Asterisks above the sequence represent residues that are highly conserved among FliJs from various species. Dots below the sequence denote residues that were unresolved in the electron density.

might form a complex similar to  $F_1$ -ATPase. We therefore mixed FliJ and FliI at various molar ratios in the presence of  $Mg^{2+}$ -ADP- $AlF_4$  and observed the mixtures by electron microscopy. The result showed that FliJ strongly affected the hexameric ring formation of FliI (Fig. 3).

When FliI and FliJ were mixed at a molar ratio of 6:1, ring formation was enhanced (Fig. 3b) approximately five-fold compared to that for FliI alone (Fig. 3a), suggesting that FliJ nucleates or stabilizes the ring formation of FliI. By contrast, at a molar ratio of 1:1, ring formation was suppressed (Fig. 3c) to about 10% of that for FliI alone (Fig. 3a), indicating that the interaction between FliI and FliJ is stronger than that between FliI subunits in the ring.

### The FliI–FliJ complex labeled with streptavidin

To examine whether FliJ forms a complex with the FliI ring, we prepared FliJ decorated with a biotin-streptavidin label, mixed it with FliI and observed the mixture by electron microscopy. We chose Ile67 of FliJ as a labeling target because its corresponding residue of the  $\gamma$  subunit is exposed on the part that sticks out of the  $\alpha_3\beta_3$  ring of  $F_1$ -ATPase. We replaced Ile67 with cysteine for labeling with biotin-PEG2-maleimide and replaced the intrinsic cysteine residue Cys32 with threonine to avoid an undesirable side reaction. FliJ(C32T/I67C) was as functional as FliJ because it restored the swarming motility of a *Salmonella*  $\Delta fliJ$  mutant to the wild-type level (data not shown). We biotinylated FliJ(C32T/I67C), mixed it with a small amount of streptavidin, and purified the FliJ–streptavidin complex by gel filtration chromatography to remove excess biotin-FliJ(C32T/I67C). From the molar ratio of FliJ and streptavidin in the complex, which was close to 1:2

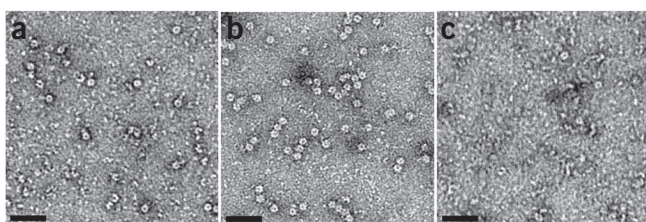


**Figure 3** Effect of FliJ on the formation of FliI rings. Negatively stained electron micrographs of FliI and FliI–FliJ mixtures. (a–c) FliI and FliJ were mixed at molar ratios of 1:0 (a), 6:1 (b) and 1:1 (c). Scale bar, 50 nm.

(Supplementary Fig. 1), we concluded that two FliJ molecules were bound to the streptavidin tetramer (FliJ<sub>2</sub>-ST<sub>4</sub>).

We mixed the FliJ<sub>2</sub>-ST<sub>4</sub> complex with FliI in the presence of  $Mg^{2+}$ -ADP- $AlF_4$  and at a FliI/FliJ molar ratio of 6:1, and observed the mixture by electron microscopy. About 80% of the FliI rings were paired with an extra density bridging the pair (Fig. 4), indicating that each FliJ subunit of the FliJ<sub>2</sub>-ST<sub>4</sub> complex associated with the ring. The density bridging the pair is likely to be streptavidin. The result confirms the strong binding of FliJ with the FliI ring.

### The FliI<sub>6</sub>FliJ complex looks just like $F_1$ -ATPase

To clarify the location of FliJ in the FliI–FliJ ring complex, we analyzed the structures of the FliI–FliJ and FliI ring particles by electron cryomicroscopy. As the orientation of the frozen-hydrated ring particles embedded in vitreous ice was strongly biased to end-on views<sup>28</sup>, three-dimensional image reconstruction was not possible. However, we aligned and averaged the end-on view images and compared the two ring particle images. The FliI ring showed a hexameric ring structure with a central hole 2 nm in diameter (Fig. 5a), as

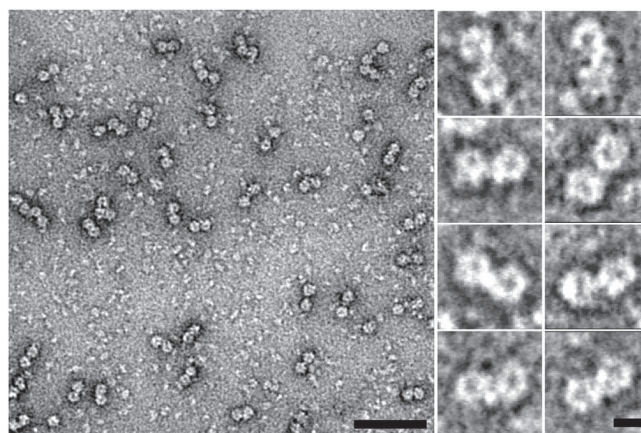


**Figure 4** Electron micrograph of the FliI–FliJ complex. Negatively stained electron micrograph of a mixture of FliI and streptavidin-labeled FliJ. Most of the rings are paired. Close up views of the ring pairs are shown on the right. The densities bridging the pair are discernible. Scale bars, 100 nm (left) and 10 nm (right).

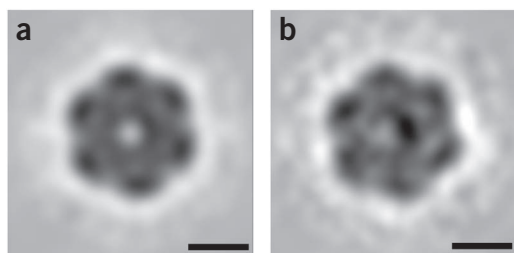


**Figure 5** Comparison of the FliI and FliI-FliJ ring complexes. (a,b) Averaged cryo-EM images of the FliI (a) and FliI-FliJ (b) ring complexes embedded in vitreous ice. Hexameric features are clear in both images, but the central hole of the FliI-FliJ ring is filled in with an off-axis density. Scale bars, 5 nm.

previously demonstrated<sup>10,11,28</sup>. The FliI-FliJ ring showed the same hexameric structure as the FliI ring, but the central hole was filled in with an extra density located clearly off-center (Fig. 5b).

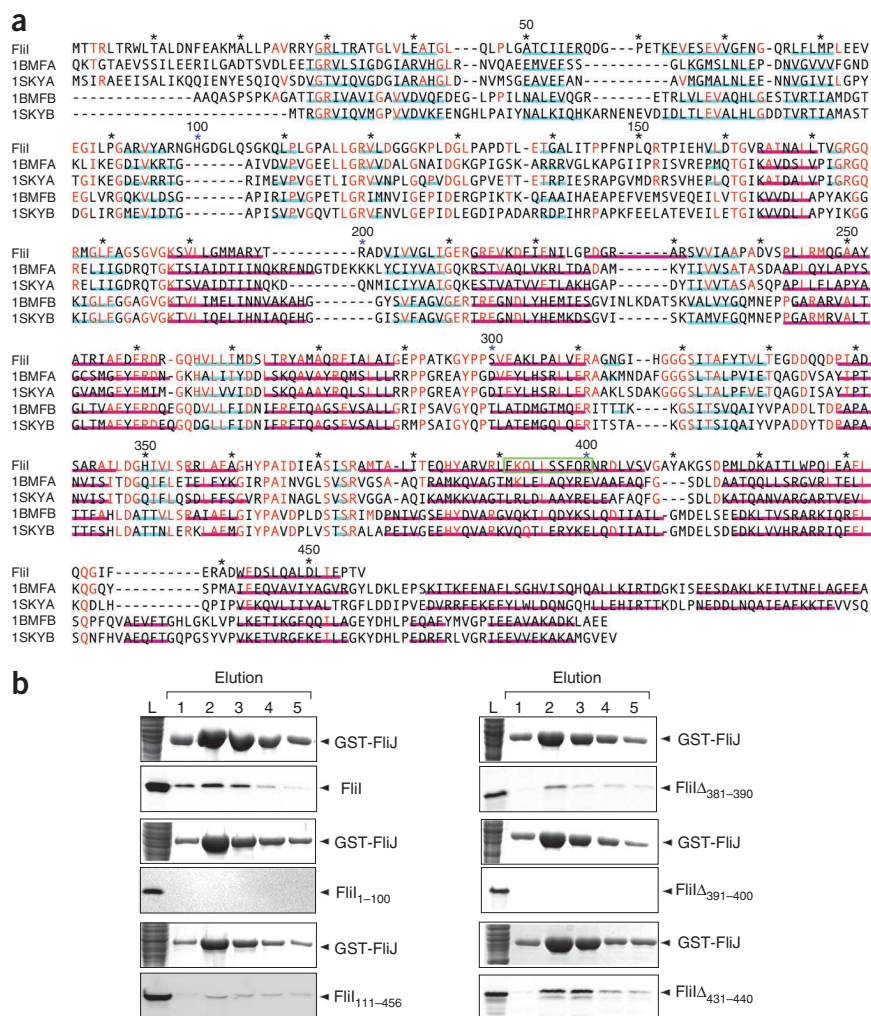
Pulldown assays by GST affinity chromatography revealed that FliJ bound to residues 391–400 (Fig. 6), which is a C-terminal region of the C1  $\alpha$ -helix of FliI<sup>9</sup>. The corresponding region of the  $\beta$  subunit is the portion with which the  $\gamma$  subunit interacts in the  $F_1$ -ATPase structure<sup>25</sup>. These observations suggest that FliJ penetrates into the central hole of the FliI hexamer ring in a similar way to the  $\gamma$  subunit penetrating into the central hole of the  $\alpha_3\beta_3$  ring in  $F_1$ -ATPase<sup>25</sup> (Fig. 7).

## DISCUSSION

The structural similarity between the FliI<sub>6</sub>FliJ ring and  $F_1$ -ATPase implies that there is a close relationship between the bacterial flagellum and  $F_0F_1$ -ATP synthase. FliH has sequence similarity to both the b and  $\delta$  subunits of  $F_0F_1$ -ATP synthase<sup>29</sup>. Moreover, the protonmotive force across the cytoplasmic membrane drives the functions of the export gate<sup>4,5</sup> and the  $F_0$  portion<sup>30</sup>. These observations suggest that the two molecular machines evolved from a common ancestral system.

Although FliJ has been postulated to be not only a general chaperone for export substrates<sup>15</sup> but also a chaperone escort protein that promotes the cycling of the substrate-specific chaperones FlgN and FliT<sup>19</sup>, our

**Figure 6** Structure-based sequence alignment of FliI and the  $\alpha$  and  $\beta$  subunits of  $F_1$ -ATPase and pulldown assay to identify the FliI region that interacts with FliJ. (a) Structure-based sequence alignment of FliI and the  $\alpha$  and  $\beta$  subunits of  $F_1$ -ATPase from bovine mitochondria (1BMFA and 1BMFB) and the thermophilic *Bacillus* PS3 (1SKYA and 1SKYB). The purple and cyan bars indicate  $\alpha$ -helices and  $\beta$ -strands, respectively. The region that interacts with FliJ is shown by the green box. Residues that are conserved between FliI and any of the  $F_1$  subunits are highlighted in red. (b) Interactions of FliJ with FliI, its fragments and deletion mutants were examined by pulldown assay using GST affinity chromatography. The eluted fractions were analyzed by both CBB staining and immunoblotting with polyclonal anti-FliI antibodies.



structure suggests a previously undescribed role for FliJ in protein export. The structural similarity between the FliI<sub>6</sub>FliJ complex and  $F_1$ -ATPase suggests that they might share a common mechanism for their distinct functions.  $F_1$ -ATPase uses a rotational mechanism to hydrolyze ATP<sup>31</sup>. The stepwise rotation of the  $\gamma$  subunit is coupled with conformational changes of the  $\alpha$  and  $\beta$  subunits that lead to sequential ATP hydrolysis at the three catalytic sites<sup>30,31</sup>. The structural similarity between the FliI<sub>6</sub>FliJ complex and  $F_1$ -ATPase suggests that FliJ might rotate within the FliI ring to promote ATP hydrolysis. Consistent with this idea, it has been reported that FliJ stimulates the ATPase activity of FliI<sup>19</sup>. We also examined the effect of FliJ on the ATPase activity of FliI. FliI is believed to self-assemble into a homohexamer in order to exert its full ATPase activity<sup>10,11</sup>. If this is the case, the highest ATPase activity would be expected when FliJ is added to FliI at a molar ratio of 1:6, where the probability of FliI<sub>6</sub>FliJ ring formation is highest, and the addition of excess FliJ should reduce the ATPase activity because the ring formation is markedly suppressed at a molar ratio of 1:1 (Fig. 3). However, the ATPase activity increased further as we increased the amount of FliJ that was added to FliI (data not shown). This result suggests that the hexamer ring structure is not indispensable for the ATPase activity of FliI. As the ATP binding site is located at the interface of two neighboring FliI subunits in the hexamer ring model<sup>9,28</sup>, like that of the  $\alpha_3\beta_3$  ring structure of  $F_1$ -ATPase<sup>25</sup>, a FliI dimer stabilized by excess FliJ might be sufficient to exert the full ATPase activity of FliI, which in turn

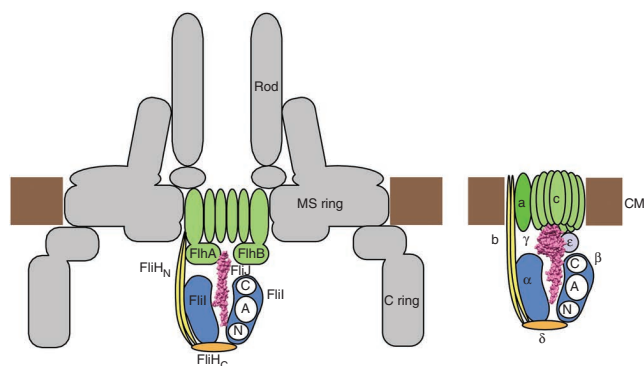


**Figure 7** Schematic diagram showing a plausible model of the FliH–FliI–FliJ complex and its relative position and orientation to the export gate.  $F_0F_1$ -ATP synthase, which is composed of the  $\alpha_3\beta_3$  ring, the  $\gamma$  and  $\epsilon$  subunits as the central stalk, the  $b$  and  $\delta$  subunits as the peripheral stalk and the  $a$  and  $c$  subunits as the transmembrane domain, is shown in the right panel as a reference. Labels C, A and N represent the C-terminal, ATPase and N-terminal domains of FliI, respectively. The flagellar basal body composed of the MS ring, C ring and rod is colored gray. CM, cytoplasmic membrane.

suggests that FliJ might not rotate to stimulate ATP hydrolysis by FliI in the ring. However, as ATP hydrolysis promotes the disassembly of the FliI ring<sup>28</sup>, presumably to allow rapid turnover of substrate delivery and insertion to the export gate<sup>4</sup>, FliJ might still have an important role in synchronizing the ATPase reactions at the six catalytic sites of the FliI ring with protein export by the export gate.

In  $F_0F_1$ -ATP synthase, the rotation of the  $c$  subunit ring in the  $F_0$  part, which is powered by protonmotive force across the cytoplasmic membrane, drives the rotation of the  $\gamma$  subunit within the  $\alpha_3\beta_3$  ring in the  $F_1$  part for ATP synthesis<sup>30</sup>. In other words, the  $\gamma$  subunit couples proton influx with the chemical synthesis of ATP. On the other hand, a specific interaction of FliJ with the export gate brought about by the FliH–FliI complex upon docking to the FlhA–FlhB platform of the gate is responsible for switching the mode of protein export from one that depends on proton influx to one that depends solely on voltage (T.M. and K.N., unpublished data). Thus, the role of FliJ in flagellar protein export might not be so closely related to that of the  $\gamma$  subunit in ATP synthesis by  $F_0F_1$ -ATP synthase, despite the extensive structural similarities between these two systems.

The genetic, structural and mechanistic similarities between the flagellar protein export apparatus and the virulence type III secretion system of pathogens have been well established<sup>1,2</sup>. Although structural information is still limited, the extensive similarities between the crystal structures of their respective ATPases, *Salmonella* FliI for flagellar protein export<sup>9</sup> and enteropathogenic *Escherichia coli* EscN for effector secretion<sup>32</sup>, emphasized the similarity between the two systems. The recently reported crystal structure of *Chlamydia trachomatis* protein CT670 (ref. 33) shows an  $\alpha$ -helical coiled-coil structure that is nearly identical to that of FliI. Although the function of CT670 is not known, its gene is located in one of the type III secretion gene clusters and the protein has been identified as a homolog of *Yersinia pestis* YscO—a core component of the Yop secretion system that has been identified as a FliJ homolog<sup>34</sup>. Therefore, the structural similarity between CT670 and FliJ provides further evidence that the mechanisms of virulence effector secretion by pathogens are similar in detail to those of flagellar protein export despite the difference in the size and shape of their basal bodies, within which the entire protein export complex is installed.

Despite the structural similarity between the type III ATPases<sup>9,32</sup> and the  $\alpha$  and  $\beta$  subunits of  $F_1$ -ATPase<sup>25</sup> and the established orientation

of the  $\alpha_3\beta_3$  ring of the  $F_1$  part relative to the transmembrane  $F_0$  part, which is connected by the  $\gamma$  subunit as the central stalk<sup>35</sup>, the orientation of the type III ATPase complex relative to the transmembrane export gate has not been firmly determined. Now with the position and orientation of FliJ in the model of the FliI<sub>6</sub>FliJ ring complex, there is little doubt that the C-terminal domain of FliI faces the membrane and is located close to the export gate, with FliJ directly connecting the FliI hexamer ring to the FlhA–FlhB platform of the gate (Fig. 7). However, to understand the mechanisms of substrate delivery and insertion to the gate, substrate specificity switching and energy coupling of the type III protein export in more detail, the structure of the entire export complex including substrate, chaperone, the ATPase complex and the transmembrane gate will be required.

## METHODS

Methods and any associated references are available in the online version of the paper at <http://www.nature.com/nsmb/>.

**Accession code.** Protein Data Bank: coordinates and structure factor for FliJ have been deposited with accession code of 3AJW.

*Note: Supplementary information is available on the Nature Structural & Molecular Biology website.*

## ACKNOWLEDGMENTS

We thank M. Shimada and K. Kazetani for technical assistance and N. Shimizu, M. Kawamoto and K. Hasegawa at SPring-8 for technical help in use of beamlines. T.I. is a research fellow of the Japan Society for the Promotion of Science. This work was supported in part by Grants-in-Aid for Scientific Research (18074006 to K.I., 22570161 to T. Minamino and 16087207 and 21227006 to K.N.) and the Targeted Proteins Research Program (TRP) from the Ministry of Education, Science and Culture of Japan.

## AUTHOR CONTRIBUTIONS

T.I. prepared samples and carried out crystallization and X-ray structure analysis. K.I. helped and supervised T.I. in X-ray crystallography. T. Minamino prepared protein expression constructs and carried out pulldown assays. T.K. helped and supervised T.I. in cryo-EM image analysis. T. Miyata collected cryo-EM images. K.N. supervised the whole project. T.I., K.I., T. Minamino and K.N. wrote the paper based on discussions with T.K. and T. Miyata.

## COMPETING FINANCIAL INTERESTS

The authors declare no competing financial interests.

Published online at <http://www.nature.com/nsmb/>.

Reprints and permissions information is available online at <http://npg.nature.com/reprintsandpermissions/>.

- Minamino, T., Imada, K. & Namba, K. Mechanisms of type III protein export for bacterial flagellar assembly. *Mol. Biosyst.* **4**, 1105–1115 (2008).
- Macnab, R.M. How bacteria assemble flagella. *Annu. Rev. Microbiol.* **57**, 77–100 (2003).
- Minamino, T. & Macnab, R.M. Components of the *Salmonella* flagellar export apparatus and classification of export substrates. *J. Bacteriol.* **181**, 1388–1394 (1999).
- Minamino, T. & Namba, K. Distinct roles of the FliI ATPase and proton motive force in bacterial flagellar protein export. *Nature* **451**, 485–488 (2008).
- Paul, K., Erhardt, M., Hirano, T., Blair, D.F. & Hughes, K.T. Energy source of flagellar type III secretion. *Nature* **451**, 489–492 (2008).
- Minamino, T., Yoshimura, S.D.J., Morimoto, Y.V., González-Pedrajo, B., Kami-ike, N. & Namba, K. Roles of the extreme N-terminal region of FliH for efficient localization of the FliH–FliI complex to the bacterial flagellar type III export apparatus. *Mol. Microbiol.* **74**, 1471–1483 (2009).
- Vogler, A.P., Homma, M., Irikura, V.M. & Macnab, R.M. *Salmonella typhimurium* mutants defective in flagellar filament regrowth and sequence similarity of FliI to  $F_0F_1$ , vacuolar, and archaeobacterial ATPase subunits. *J. Bacteriol.* **173**, 3564–3572 (1991).
- Fan, F. & Macnab, R.M. Enzymatic characterization of FliI: an ATPase involved in flagellar assembly in *Salmonella typhimurium*. *J. Biol. Chem.* **271**, 31981–31988 (1996).
- Imada, K., Minamino, T., Tahara, A. & Namba, K. Structural similarity between the flagellar type III ATPase FliI and  $F_1$ -ATPase subunits. *Proc. Natl. Acad. Sci. USA* **104**, 485–490 (2007).

10. Claret, L., Susannah, C.R., Higgins, M. & Hughes, C. Oligomerisation and activation of the FliI ATPase central to bacterial flagellum assembly. *Mol. Microbiol.* **48**, 1349–1355 (2003).
11. Minamino, T. *et al.* Oligomerization of the bacterial flagellar ATPase FliI is controlled by its extreme N-terminal region. *J. Mol. Biol.* **360**, 510–519 (2006).
12. Minamino, T. & Macnab, R.M. FliH, a soluble component of the type III flagellar export apparatus of *Salmonella*, forms a complex with FliI and inhibits its ATPase activity. *Mol. Microbiol.* **37**, 1494–1503 (2000).
13. Lane, M.C., O'Toole, P.W. & Moore, S.A. Molecular basis of the interaction between the flagellar export proteins FliH and FliI from *Helicobacter pylori*. *J. Biol. Chem.* **281**, 508–517 (2006).
14. Minamino, T., González-Pedrajo, B., Kihara, M., Namba, K. & Macnab, R.M. The ATPase FliI can interact with the type III flagellar protein export apparatus in the absence of its regulator FliH. *J. Bacteriol.* **185**, 3983–3988 (2003).
15. Minamino, T., Chu, R., Yamaguchi, S. & Macnab, R.M. Role of FliJ in flagellar protein export in *Salmonella*. *J. Bacteriol.* **182**, 4207–4215 (2000).
16. Minamino, T. & Macnab, R.M. Interactions among components of the *Salmonella* flagellar export apparatus and its substrates. *Mol. Microbiol.* **35**, 1052–1064 (2000).
17. Fraser, G.M., González-Pedrajo, B., Tame, J.R. & Macnab, R.M. Interactions of FliJ with the *Salmonella* type III flagellar export apparatus. *J. Bacteriol.* **185**, 5546–5554 (2003).
18. González-Pedrajo, B., Minamino, T., Kihara, M. & Namba, K. Interactions between C ring proteins and export apparatus components: a possible mechanism for facilitating type III protein export. *Mol. Microbiol.* **60**, 984–998 (2006).
19. Evans, L.D., Stafford, G.P., Ahmed, S., Fraser, G.M. & Hughes, C. An escort mechanism for cycling of export chaperones during flagellum assembly. *Proc. Natl. Acad. Sci. USA* **103**, 17474–17479 (2006).
20. Imada, K., Minamino, T., Kinoshita, M., Furukawa, Y. & Namba, K. Structural insight into the regulatory mechanisms of interactions of the flagellar type III chaperone FliT with its binding partners. *Proc. Natl. Acad. Sci. USA* **107**, 8812–8817 (2010).
21. Bange, G. *et al.* FlhA provides the adaptor for coordinated delivery of late flagella building blocks to the type III secretion system. *Proc. Natl. Acad. Sci. USA* **107**, 11295–11300 (2010).
22. Saijo-Hamano, Y. *et al.* Structure of the cytoplasmic domain of FlhA and implication for flagellar type III protein export. *Mol. Microbiol.* **76**, 260–268 (2010).
23. Ibuki, T., Shimada, M., Minamino, T., Namba, K. & Imada, K. Crystallization and preliminary X-ray analysis of FliJ, a cytoplasmic component of the flagellar type III protein-export apparatus from *Salmonella sp.* *Acta Crystallogr.* **F65**, 47–50 (2009).
24. Holm, L., Kääriäinen, S., Rosenström, P. & Schenkel, A. Searching protein structure databases with DaliLite v.3. *Bioinformatics* **23**, 2780–2781 (2008).
25. Abrahams, J.P., Leslie, A.G., Lutter, R. & Walker, J.E. Structure at 2.8 Å resolution of F<sub>1</sub>-ATPase from bovine heart mitochondria. *Nature* **370**, 621–628 (1994).
26. Gibbons, C., Montgomery, M.G., Leslie, A.G. & Walker, J.E. The structure of the central stalk in bovine F<sub>1</sub>-ATPase at 2.4 Å resolution. *Nat. Struct. Biol.* **7**, 1055–1061 (2000).
27. Numoto, N., Hasegawa, Y., Takeda, K. & Miki, K. Inter-subunit interaction and quaternary rearrangement defined by the central stalk of prokaryotic V<sub>1</sub>-ATPase. *EMBO Rep.* **10**, 1228–1234 (2009).
28. Kazetani, K., Minamino, T., Miyata, T., Kato, T. & Namba, K. ATP-induced FliI hexamerization facilitates bacterial flagellar protein export. *Biochem. Biophys. Res. Commun.* **388**, 323–327 (2009).
29. Pallen, M.J., Bailey, C.M. & Beatson, S.A. Evolutionary links between FliH/YscL-like proteins from bacterial type III secretion systems and second-stalk components of the FoF<sub>1</sub> and vacuolar ATPases. *Protein Sci.* **15**, 935–941 (2006).
30. Yoshida, M., Muneyuki, E. & Hisabori, T. ATP synthase—a marvellous rotary engine of the cell. *Nat. Rev. Mol. Cell Biol.* **2**, 669–677 (2001).
31. Noji, H., Yasuda, T., Yoshida, M. & Kinoshita, K. Direct observation of the rotation of F<sub>1</sub>-ATPase. *Nature* **386**, 299–302 (1997).
32. Zarivach, R., Vuckovic, M., Deng, W., Finlay, B.B. & Strynadka, N.C.J. Structural analysis of a prototypical ATPase from the type III secretion system. *Nat. Struct. Mol. Biol.* **14**, 131–137 (2007).
33. Lorenzini, E. *et al.* Structure and protein-protein interaction studies on *Chlamydia trachomatis* protein CT670 (YscO homolog). *J. Bacteriol.* **192**, 2746–2756 (2010).
34. Payne, P.L. & Straley, S.C. YscO of *Yersinia pestis* is a mobile core component of the Yop secretion system. *J. Bacteriol.* **180**, 3882–3890 (1998).
35. Stock, D., Leslie, A.G.W. & Walker, J.E. Molecular architecture of the rotary motor in ATP synthase. *Science* **286**, 1700–1705 (1999).
36. Ashkenazy, H., Erez, E., Martz, E., Pupko, T. & Ben-Tal, N. ConSurf 2010: calculating evolutionary conservation in sequence and structure of proteins and nucleic acids. *Nucleic Acids Res.* **38**, W529–W533 (2010).

## ONLINE METHODS

**Bacterial strains, plasmids and media.** *Salmonella* and *E. coli* strains and plasmids used in this study are listed in **Supplementary Table 1**. Luria broth (LB) and soft tryptone agar plates were prepared as described<sup>16</sup>.

**Preparation and crystallization of FliJ.** Details of expression, purification and crystallization of *Salmonella* FliJ have been described<sup>23</sup>. Briefly, hexagonal  $P6_522$  crystals of FliJ with unit cell dimensions  $a = b = 52.9 \text{ \AA}$ ,  $c = 193.6 \text{ \AA}$  and  $\gamma = 120^\circ$  were grown from a solution containing PEG300 and NaCl by the sitting-drop vapor diffusion method. The mercury derivative of FliJ was prepared and crystallized as described<sup>23</sup>.

**Data collection and structure determination.** X-ray diffraction data were collected with a wavelength of  $1.008 \text{ \AA}$  for the mercury derivative at synchrotron beamline BL41XU of SPring-8 (Harima, Japan) with the approval of the Japan Synchrotron Radiation Research Institute (JASRI) (proposal nos. 2007A1657 and 2008A1392). The statistics of the data have been described<sup>23</sup>. The data were processed with MOSFLM<sup>37</sup> and scaled with SCALA<sup>38</sup>. The initial single-wavelength anomalous dispersion (SAD) phase was calculated from the anomalous data of a mercury derivative crystal using SOLVE<sup>39</sup> and improved by density modification using DM<sup>38</sup>. The atomic model was constructed with COOT<sup>40</sup> and refined to  $2.1 \text{ \AA}$  with CNS<sup>41</sup>. During the refinement process, manual modification was performed by using an 'omit map'. The refinement converged to an  $R$  factor of 23.3% and a free  $R$  factor of 25.5%. The Ramachandran plot showed that 95.2% and 4.8% of residues were located in the most favorable and allowed regions, respectively. Structural refinement statistics are summarized in **Table 1**.

**Preparation and purification of FliI.** A 30-ml overnight culture of *E. coli* strain BL21(DE3)pLysS carrying pMM1771, which encodes FliI with an N-terminal hexahistidine (His-FliI) followed by a thrombin-cleavage site on pTrc99A (GE Healthcare), was inoculated into 1 liter of LB medium containing  $50 \mu\text{g ml}^{-1}$  ampicillin and  $30 \mu\text{g ml}^{-1}$  chloramphenicol. Cells were grown at 296 K until the culture density reached an  $\text{OD}_{600}$  of 0.6. Expression of His-FliI was induced with isopropyl-1-thio  $\beta$ -D-galactopyranoside (IPTG) at a final concentration of 0.1 mM. Overnight culture was centrifuged ( $6,400\text{g}$ , 10 min, 277 K) and the cells were stored at 193 K. The cells were thawed, suspended in a binding buffer (50 mM Tris-HCl pH 8.0, 500 mM NaCl, 80 mM imidazole) with a tablet of Complete protease-inhibitor cocktail (Boehringer Mannheim), and sonicated (ASTRASON model XL2020 sonicator, Misonix Inc.). After centrifugation (19,000g, 20 min, 277 K), the supernatant was loaded onto a HiTrap chelating column (GE Healthcare) equilibrated with the binding buffer. Proteins were eluted using a linear gradient of imidazole. Fractions containing His-FliI were kept with 50 units of thrombin (GE Healthcare) at 277 K overnight and applied to a HiLoad Superdex 75 (26/60) column (GE Healthcare) in 50 mM Tris-HCl pH 8.0, 150 mM NaCl.

**Preparation and purification of FliJ mutants.** The mutant variants of FliJ (FliJ(C32T) and FliJ(C32T/I67C)) were generated by QuikChange site-directed mutagenesis (Stratagene). Coding and antisense primers containing a single mutagenic site were used for PCR amplification. The mutant proteins were expressed in BL21(DE3)pLysS and purified by the same protocol used for FliJ<sup>23</sup>.

**In vitro reconstruction of the FliI ring and electron microscopy.** Purified FliI or mixtures of FliI and FliJ(C32T) at various molar ratios were incubated in 35 mM Tris-HCl (pH 8.0), 113 mM NaCl, 0 or 1 mM DTT, 5 mM ADP, 5 mM

$\text{AlCl}_3$ , 15 mM NaF, 5 mM  $\text{MgCl}_2$  and  $100 \mu\text{g ml}^{-1}$  acidic phospholipids at 310 K for a few minutes. The final concentration of FliI in each solution was adjusted to  $50 \mu\text{g ml}^{-1}$ . Samples were applied to carbon-coated copper grids and negatively stained with 2% (w/v) uranyl acetate. Micrographs were recorded at a magnification of  $\times 35,000$  with a JEM-1011 transmission electron microscope (JEOL) operated at 100 kV.

**Pulldown assays by GST affinity chromatography.** Pulldown assays by GST affinity chromatography were carried out as described<sup>6</sup>. The mixture of the soluble fractions prepared from SJW1368 ( $\Delta$ fliHDC-cheW mutant) expressing GST-FliJ with those from SJW1368 producing His-FliI, His-FliI(1–100), His-FliI(111–456), FliI $\Delta$ (381–390), FliI $\Delta$ (391–400) and FliI $\Delta$ (431–440) were loaded onto a GST column. After extensive washing, proteins were eluted with a buffer containing 10 mM reduced glutathione.

**Preparation of FliJ labeled with streptavidin.** Crude FliJ(C32T/I67C) with His tag was mixed with 1 mM biotin-PEG2-maleimide (Thermo), was loaded on a HiTrap chelating column and incubated for 3 h at room temperature. Then, the biotinylated FliJ(C32T/I67C) was purified by the same method used for FliJ<sup>23</sup> and mixed with a small amount of streptavidin (Thermo). The streptavidin-labeled FliJ(C32T/I67C) was purified with a HiLoad Superdex 75 (26/60) column in 50 mM Tris-HCl pH 8.0 and 150 mM NaCl. The molar ratio of streptavidin and FliJ(C32T/I67C) in their complex was determined to be 2.1:1 as described in the legend of **Supplementary Figure 1**. Because streptavidin forms a stable tetramer, we identified the complex as FliJ<sub>2</sub>ST<sub>4</sub>.

**Electron cryomicroscopy and image analysis.** Sample grids for electron cryomicroscopy were prepared by applying a 4- $\mu\text{l}$  protein solution ( $150 \mu\text{g ml}^{-1}$ ) onto a holey carbon grid (Quantifoil R0.6/1.3, Quantifoil Micro Tools), which had been glow-discharged in a weak vacuum for 20 s immediately before use. The grids were blotted for 3 s, quick-frozen in liquid ethane using Vitrobot (FEI) and transferred to a liquid nitrogen storage capsule. Images were recorded using a TVIPS 4K  $\times$  4K CCD camera on a JEM-3200FSC electron microscope (JEOL), equipped with a liquid-helium cooled specimen stage, an  $\Omega$ -type energy filter and a field-emission electron gun operated at an accelerating voltage of 200 kV. Micrographs were recorded at 50 K with a magnification of  $\times 140,000$ , corresponding to  $1.07 \text{ \AA}$  per pixel. Focal pairs of micrographs were recorded at a defocus between 1.5 and 2.5  $\mu\text{m}$  for the first micrograph and at a defocus between 3.5 and 5.5  $\mu\text{m}$  for the second, both with an electron dose of  $40 e^- \text{ \AA}^{-2}$ , and were merged using the FOCALPAIR<sup>42,43</sup>. The defocus amplitude, envelope and noise values were determined using CTFIT<sup>42</sup>. Micrographs showing astigmatism or drift appreciable by eyes were discarded. The particle images were selected with BOXER<sup>42</sup>, and the boxed particle images were aligned and classified using the REFINE2D.PY<sup>42</sup>.

37. Leslie, A.G.W. Joint CCP4 and ESF/EACMB newsletter on protein. *Protein Crystallogr* **26**, 27–33 (1992).
38. Collaborative Computational Project. Number 4, The CCP4 suite: programs for protein crystallography. *Acta Crystallogr.* **D50**, 760–763 (1994).
39. Terwilliger, T.C. & Berendzen, J. Automated MAD and MIR structure solution. *Acta Crystallogr.* **D55**, 849–861 (1999).
40. Emsley, P. & Cowtan, K. Coot: model-building tools for molecular graphics. *Acta Crystallogr.* **D60**, 2126–2132 (2004).
41. Brünger, A.T. *et al.* Crystallography & NMR system: a new software suite for macromolecular structure determination. *Acta Crystallogr.* **D54**, 905–921 (1998).
42. Ludtke, S.J., Baldwin, P.R. & Chiu, W. EMAN: Semiautomated software for high-resolution single-particle reconstructions. *J. Struct. Biol.* **128**, 82–97 (1999).
43. Ludtke, S.J. & Chiu, W. Focal pair merging for contrast enhancement of single particles. *J. Struct. Biol.* **144**, 73–78 (2003).